PCCP

PAPER

View Article Online
View Journal | View Issue

Cite this: *Phys. Chem. Chem. Phys.*, 2022, **24**, 8217

Photoinduced water–chromophore electron transfer causes formation of guanosine photodamage†

Mikołaj J. Janicki, *[a] Rafał Szabla, *[a] Jiří Šponer[bc] and Robert W. Góra *[a]

Received 17th February 2022,
Accepted 4th March 2022

DOI: 10.1039/d2cp00801g

rsc.li/pccp

UV-induced photolysis of aqueous guanine nucleosides produces 8-oxo-guanine and Fapy-guanine, which can induce various types of cellular malfunction. The mechanistic rationale underlying photodestructive processes of guanine nucleosides is still largely obscure. Here, we employ accurate quantum chemical calculations and demonstrate that an excited-state non-bonding interaction of guanosine and a water molecule facilitates the electron-driven proton transfer process from water to the chromophore fragment. This subsequently allows for the formation of a crucial intermediate, namely guanosine photohydrate. Further (photo)chemical reactions of this intermediate lead to the known products of guanine photodamage.

Introduction

Ultraviolet-driven chemical reactions in nucleic acid components could entail irreversible damage to their molecular structure, and consequently may result in undesirable mutagenic processes in biological systems.[1–7] Accumulation of such alterations in the genome can induce cellular malfunction, tumorigenesis, and even cell death.[8,9] Therefore, understanding the photochemical mechanisms directly enabling the formation of DNA/RNA lesions is a fundamental issue for cellular biology and disease prevention. 8-oxo-guanine and 2,6-diamino-4-oxo-5-formamidopyrimidine (Fapy-guanine) are among the most frequent DNA/RNA photolesions, which are produced upon UV excitation of guanine nucleosides in relative yields strongly dependent on the local chemical environment.[10–14] However, despite considerable efforts to scrutinize the molecular mechanisms underlying UV-induced damage of pyrimidine nucleobases,[15–21] photochemical processes causing generation of guanine nucleoside lesions (such as 8-oxo-guanine or Fapy-guanine) are still obscure. In this paper, we provide a plausible explanation based on the reinterpretation of available experimental data and our state-of-the-art *ab initio* calculations.

In recent decades, the photodynamics of guanine nucleosides was extensively investigated through time-resolved (TR) spectroscopic measurements that were often supplemented by quantum-chemical calculations.[22–28] Joint experimental–theoretical studies demonstrated that the photoinduced dynamics of aqueous guanine nucleosides is characterized by sub-picosecond excited-state lifetimes that were assigned to the population of the $^1\pi\pi^*$ excited state. Indeed, the proposed ballistic photorelaxation pathways most likely enable the observed ultrafast deactivation of nucleosides, but this does not explain the origin of guanine photolesions. In addition to the recorded short-lived signals, a complementary longer-lived and weakly-emissive ($\sim$2 ps) excited state has been identified and tentatively assigned to the charge-transfer $^1\pi\sigma^*$ excited state.[22,23] However, the accessibility of such a repulsive state in guanine nucleosides seems rather unlikely as there are no distinctive signatures in the TR absorption spectra[22,23] originating from solvated electrons (expected in the range of 600–700 nm) that could be produced through the population of the $^1\pi\sigma^*$ electronic state.[29] Importantly, this puzzling excited state efficiently quenches the strongly emissive $^1\pi\pi^*$ states and its lifetime varies in different polar solvents such as water and methanol.[22,23]

Recent advances in mechanistic studies of aqueous photochemistry of pyrimidine and purine nucleobases[30–32] have shown that the dark $^1n\pi^*$ excited states can serve as a doorway to UV-induced water-to-chromophore electron transfer. This process is enabled by an excited-state interaction of the lone electron pairs of a heteroatom in the aromatic ring and the neighbouring water molecule. Consequently, the photoinduced electron transfer and the subsequent proton transfer may lead

[a] *Faculty of Chemistry, Wrocław University of Science and Technology, Wybrzeże Wyspiańskiego 27, 50-370, Wrocław, Poland. E-mail: mikolaj.janicki@pwr.edu.pl, rafal.szabla@pwr.edu.pl, robert.gora@pwr.edu.pl*
[b] *Institute of Biophysics of the Czech Academy of Sciences, Královopolská 135, 61265 Brno, Czech Republic*
[c] *National Centre for Biomolecular Research, Faculty of Science, Masaryk University, Kamenice 5, 625 00, Brno, Czech Republic*

† Electronic supplementary information (ESI) available: Computational procedures, conformational analysis, and characteristics of excited-state crucial points. See DOI: 10.1039/d2cp00801g

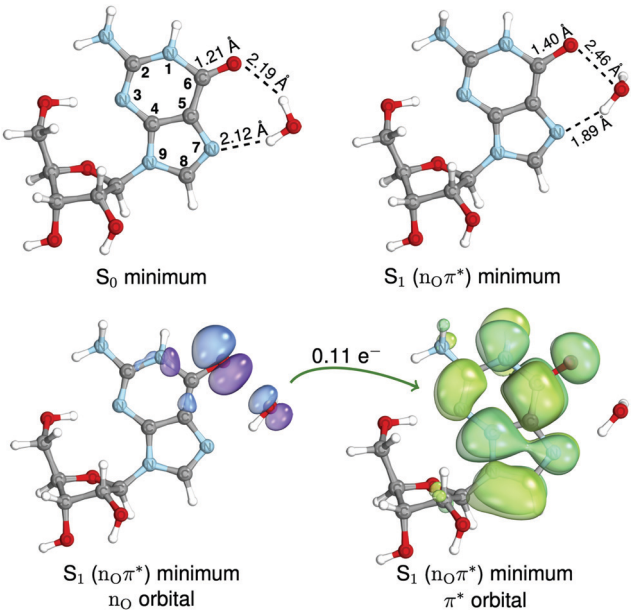

Fig. 1 The geometries of the **Guo-H_2O** complex corresponding to the S_0 and S_1 ($n_O\pi^*$) minimum-energy structures are shown in the first row. Below, the molecular orbitals involved in the S_1 ($n_O\pi^*$) transition are shown, which demonstrate a charge-transfer character of the process in which 0.11 e^- is transferred from the water molecule to the nucleoside. The assumed numbering of atoms and the relevant distances between atoms are indicated.

to the formation of reactive hydroxyl radicals causing damage to DNA/RNA bases.[30–32]

Our working hypothesis is that the population of the dark $^1n_O\pi^*$ state in a complex of guanine nucleoside and an explicit water molecule (**Guo-H_2O**, see Fig. 1) is attainable through the excited-state intermolecular C6–O$\cdots$$OH_2$ chalcogen bonding interaction, which triggers the long-sought photochemical pathway to the formation of both 8-oxo-guanosine and Fapy-guanosine.

The results of our quantum-chemical calculations are supported by comparison with previously recorded time-resolved femtosecond transient absorption spectra obtained for aqueous guanine nucleosides.[22,23]

Computational methods

To find the most stable structures of nucleosides in an aqueous environment, the conformational space was explored using the Conformer-Rotamer Ensemble Sampling Tool[33] (CREST) at the semi-empirical GFN2-xTB[34] level of theory. The exploration of the conformational space was performed using the iMTD-GC scheme along with the analytical linearized Poisson–Boltzmann (ALPB) implicit solvent model representing the water solvent. The equilibrium ground-state geometries and harmonic vibrational frequencies of the lowest-energy conformer were then obtained using Kohn–Sham density functional theory (KS-DFT) employing the range-separated hybrid ωB97X-D functional[35] and the def2-TZVPP[36] basis set. The KS-DFT calculations were performed using the Gaussian 16[37] package.

Vertical excitation energies were obtained using the spin-component scaled variant[38] of the second-order algebraic diagrammatic construction[39,40] [SCS-ADC(2)] with the cc-pVTZ basis set[41] [SCS-ADC(2)/cc-pVTZ], assuming the equilibrium ground-state structures optimized as described above. The orbital character of each electronic transition was assigned based on natural transition orbitals (NTOs). The estimation of solvent-to-chromophore transferred charge was obtained using the one-electron transition density matrix (1TDM) and the Löwdin style analysis. Tg 1TDM analysis was performed employing the TheoDore[42] 2.4 package. Excited-state minimum-energy structures were located at the SCS-ADC(2)/cc-pVTZ level of theory. The optimization of minimum-energy crossing points (MECPs) between two electronic states was performed employing the sequential penalty constrained function implemented by Levine *et al.*[43] in the CIOpt package. To locate MECPs, the energies and analytical nuclear gradients for the electronic excited and ground states were computed at the SCS-ADC(2) and SCS-MP2 levels, respectively, with the cc-pVTZ basis set.

To verify excited-state minimum energy structures and the S_1/S_0 state crossing obtained using the single reference method, we optimized these critical excited-state geometries with the extended multi-state complete active space second-order perturbation theory[44,45] (XMS-CASPT2), employing the state-averaged complete active space self-consistent field (SA-CASSCF) method with the cc-pVDZ basis set. To locate the S_1 ($n_O\pi^*$) minimum-energy structure at the XMS-CASPT2 level, the complete active space (CAS) was composed of molecular orbitals (MOs) having natural orbital occupations in the range of 0.02–1.98,[46] augmented by n_O, σ_O, and σ_O^* orbitals to facilitate the C6–O$\cdots$$OH_2$ excited-state interaction in the S_1 ($n_O\pi^*$) state and the possible elongation of the carbonyl bond. Consequently, the active space was built out of one σ_O, three π and one n_O occupied MOs along with three π^* and one σ_O^* virtual MOs (10 electrons in 9 orbitals, shown in Fig. S10, ESI†). The SA-CASSCF wave function was averaged over four lowest-lying electronic states. The optimization of the S_1/S_0 minimum-energy conical intersection was performed assuming the CAS constructed of the π_O, two π, two n_O, and four π^* MOs (10 electrons in 9 orbitals, shown in Fig. S11, ESI†). In the latter calculations, we included two lone electron pair n_O orbitals in the CAS to allow for an appropriate description of the hydroxyl radical. The SA-CASSCF wave function was averaged over three lowest-lying electronic states. The vertical shift, *i.e.*, the empirical correction applied to the zeroth-order Hamiltonian, was equal to 0.4 Hartree, and the XMS-CASPT2 calculations were conducted using the BAGEL 1.2.0[47] package. To estimate the emission energy of the S_1 ($n_O\pi^*$) structure, SCS-ADC(2) theory was used alongside the conductor-like screening model (COSMO) as an implicit solvent, assuming the equilibrium solvation limit for the S_1 excited state, and SCS-ADC(2) calculations were performed using the TURBOMOLE 7.3[48] package.

Excited-state absorption spectra of S_1 minimum-energy structures were simulated based on calculations of 14 excited states, which provided the excitation energies and corresponding oscillator strengths at the SCS-ADC(2)/cc-pVTZ level of theory.

Absorption lineshapes, assuming the full width at half-maximum equal to 3000 cm^{-1}, were generated using the GaussSum 3.0[49] program.

The potential energy (PE) profiles for the singlet electron-driven proton transfer (EDPT) photorelaxation pathway were computed at the SCS-ADC(2)/cc-pVTZ level of theory using the key excited-state structures, namely S_2/S_1 and S_1/S_0 MECPs and the S_1 minimum-energy structure. The PE profiles between the Franck–Condon region and the S_1 minimum were obtained by single-point calculations of intermediate geometries constructed by the image dependent pair potential (IDPP) interpolation[50] between the optimized geometries. To show PE profiles between the S_1 minimum and S_1/S_0 MECP, relaxed excited-state geometry optimization was performed constraining the H–O bond length (0.97–1.27 Å) in the N7···H–OH moiety at the SCS-ADC(2)/cc-pVTZ level. The IDPP interpolation was also employed to obtain intermediate structures between the optimized constrained S_1 geometry, having a H–O bond distance of 1.27 Å, and the S_1/S_0 MECP. The optimization of ground-state structures of photo-products was performed using the ωB97X-D functional[35] with the def2-TZVPP[51] basis set. Relative energies of the photo-products were determined using the polarizable continuum model (PCM) as an implicit solvent model, assuming their gas-phase optimized geometries. The IDPP interpolations were performed using the Orca 4.2.1.[52] package.

Results and discussion

Ground-state structures

Based on the conformational analysis of **Guo**, performed using the semi-empirical GFN2-xTB method[34] (see Fig. S1 in the ESI†), we found that the structure having the *syn* orientation of the nucleobase and the C2′-*endo* arrangement of the sugar ring is energetically preferred in an aqueous environment. Our results agree with previous molecular dynamics simulations of guanosine monophosphate that showed dominant population of the syn-like conformer (occurring in 93% of simulations).[26] It is worth noting that the *syn* orientation enables the formation of the OH···N3 hydrogen bond between the sugar moiety and the nucleobase (see Fig. 1). This intramolecular hydrogen bond was previously shown to allow for an excited-state forward–backward proton transfer mechanism between the nucleobase and sugar, which could serve as a radiationless deactivation channel of excited purine nucleosides.[53–55]

We added a single explicit water molecule to the selected structure of **Guo**, to saturate hydrogen bonds with potentially photoreactive sites of the guanine moiety, namely, the C6–O and N7 atoms. Finally, we optimized the ground-state geometry of this **Guo-H_2O** complex (see Fig. 1) using the ωB97X-D/def2-TZVPP method. The resulting equilibrium S_0 geometry of the **Guo-H_2O** complex has the water molecule lying in the plane of the aromatic purine ring, to which it is attached by two hydrogen bonds with the carbonyl group (2.19 Å) and the N7 atom (2.12 Å; see Fig. 1). We expect that upon UV excitation, the C6–O···H_2O hydrogen bond would break and thus facilitate the accessibility of the $^1n_O\pi^*$ dark state.[31] It is worth adding that we constructed a similar water complex with deoxyguanosine (**dGuo-H_2O**, see ESI†), and the optimization procedure yielded a virtually identical structure.

Vertical excitation energies

We further computed the vertical excitation energies (shown in Table 1) of the low-lying electronically excited states in the Franck–Condon region of **Guo-H_2O** using the SCS-ADC(2)/cc-pVTZ method. The obtained data show that the absorption of UV photons can result in population of the two locally-excited (LE) $^1\pi\pi^*$ states (at 5.13 and 5.76 eV) marked by relatively high oscillator strengths (see Fig. S3 in ESI†). The population of either of the $^1\pi\pi^*$ states enables dissipation of the excitation energy through puckering of the aromatic ring and out-of-plane motion of the amino group. These ring-puckering pathways allow for ultrafast non-destructive deactivation to the electronic ground state and are often referred to as ballistic photorelaxation mechanisms.[22,26,56,57] However, in the context of this study, we focus on the $^1n_O\pi^*$ excitation at 5.63 eV (Table 1) that is characterized by a transition from the non-bonding lone electron pair molecular orbital located on the carbonyl oxygen atom that is also partially localized on the water molecule (see Fig. S3 in ESI†). The $^1n_O\pi^*$ state in the Franck–Condon region exhibits a moderate charge-transfer (CT) character, associated with the donation of 0.06 e^- from the water molecule to the chromophore moiety. We expect that even more pronounced water-to-chromophore electron transfer would occur on the $^1n_O\pi^*$ potential energy (PE) surface due to geometry relaxation. It is worth noting that the photophysical properties of **dGuo-H_2O** (see Table S1 in the ESI†) are entirely consistent with those of the **Guo-H_2O** system.

Water-to-chromophore electron transfer

To explore the $^1n_O\pi^*$ potential energy surface, we performed excited-state geometry optimization for the **Guo-H_2O** complex. The located S_1 ($n_O\pi^*$) minimum-energy structure (see the upper panel in Fig. 1) shows an intriguing intermolecular chalcogen bonding interaction between the oxygen atoms of the chromophore and the water molecule (C6–O···OH_2), with an O···O distance of 2.46 Å. To the best of our knowledge, such a UV-induced intermolecular interaction between two oxygen atoms

Table 1 Vertical excitations energies (in eV) of **Guo-H_2O** and **Guo-OH** obtained at the SCS-ADC(2) level of theory using the cc-pVTZ and aug-cc-pVDZ basis sets, respectively. These equilibrium ground-state structures were found using the ωB97X-D/def2-TZVPP method

State/transition		E_{exc} [eV]	f_{osc}	λ [nm]
		Guo-H_2O		
S_1	$\pi\pi^*_{LE}$	5.13	1.71×10^{-1}	241.7
S_2	$n_O\pi^*$	5.63	1.37×10^{-4}	220.2
S_3	$\pi\pi^*_{LE}$	5.76	3.26×10^{-1}	215.3
		Guo-OH		
S_1	$\pi\pi^*_{LE}$	4.08	1.80×10^{-1}	303.9
S_2	$\pi\sigma^*$	4.23	1.95×10^{-2}	293.1
S_3	$\pi\sigma^*$	4.52	1.81×10^{-2}	274.3

has not been reported in the literature so far, although it resembles other excited-state water-to-chromophore contacts reported previously.[30,31,58] However, the intramolecular O···O chalcogen bonding in the electronic ground state has already been confirmed experimentally by Fellowes *et al.*[59] in oxime. The excited-state chalcogen bonding complex is stabilized through the interaction of the non-bonding orbitals n_O located on the carbonyl group and the H_2O molecule (see the bottom panel in Fig. 1). The formation of the O···O chalcogen contact entails the elongation of the C6–O bond by 0.2 Å and a higher degree of charge transfer (0.11 e^- in the S_1 minimum) when compared to the Franck–Condon region. In addition, there is a slight pyramidalization of the N1 atom and an out-of-plane distortion of the amino group at the C2 position of the purine ring. We also found the analogous S_1 ($n_O\pi^*$) minimum-energy geometry for **dGuo-H_2O** (see Fig. S4 in ESI†) that closely resembles the charge-transfer mechanism described for **Guo-H_2O**.

Interestingly, previous TR infrared experiments revealed that the carbonyl group actively contributes to the energy dissipation process of UV-excited guanine nucleosides and that the C6–O bond vibrations are also coupled to the vibrational modes of the solvent.[24,25] Thus, the elongation of the C6–O bond associated with the described chalcogen O···O intermolecular interaction (Fig. 1) serves as a reasonable mechanistic rationale for this experimental observation.

The formation of the O···O chalcogen contact in the S_1 minimum substantially lowers the vertical energy gap between the S_1 ($n_O\pi^*$) and S_0 states, which amounts to merely 2.56 eV in the corresponding S_1 minimum. Cheng *et al.*[23] demonstrated that in the photodynamics of guanine nucleosides, the puzzling longer-lived excited state exhibits a very weak broadband emission (420–600 nm) with a maximum at 520 nm. The SCS-ADC(2) S_1 ($n_O\pi^*$) minimum can be associated with the weak emission due to its dipole-forbidden character, and an energy gap of 2.56 eV (484 nm) agrees very well with the experimentally determined fluorescence spectrum. We further validated this result by calculations involving the COSMO solvent model of bulk water. The results of COSMO/SCS-ADC(2)/cc-pVTZ calculations indicate that the S_1 minimum-energy structure is only slightly destabilized by $\sim$0.01 eV in bulk water and that the emission wavelength and the oscillator strength of S_1 ($n_O\pi^*$) amount to 482 nm (or 2.57 eV) and 1.92×10^{-4}, respectively. Therefore, we postulate that the previously recorded experimental weak emission band could be another fingerprint of the discussed dark $^1n_O\pi^*$ state.

Excited-state absorption spectra

To further support our hypothesis about the population of the $^1n_O\pi^*$ excited state during the photodynamics of guanine nucleosides, we simulated excited-state absorption spectra (ESA) that are overlayed with experimental transient absorption spectra, taken from previous studies,[22,23] and are shown in Fig. 2. For this purpose, we used the S_1 ($n_O\pi^*$) minimum-energy structures of the **Guo-H_2O** complex (Fig. 1) and the analogous complex of deoxyguanosine with one water molecule (**dGuo-H_2O**, Fig. S4 in ESI†).

The experimental and simulated excited-state absorption spectra having maxima at 298 and 325 nm, respectively, exhibit reasonably consistent lineshapes in the range of 290–350 nm, which confirms that the UV-induced O···O chalcogen bonding structure may indeed be attainable in the photodynamics of guanine nucleosides.[22,23] The discrepancies between the positions and shapes of the simulated and experimental absorption bands are expected and can be ascribed to the following reasons. First, the ESA spectra for the S_1 ($n_O\pi^*$) structures are simulated using model systems containing a single water molecule that do not allow to fully take into account the effects of bulk water on the position of the absorption bands, and thereby the discussed maxima differ by 27 nm. Second, the recorded TA bands possess two different spectral regions, namely below and above 350 nm, which are fingerprints of different photochemical processes. The acquired TA spectrum in the range of 350–500 nm has been previously ascribed to the $^1\pi\pi^*$ deactivation channels.[22,23] Since our simulated ESA spectra are obtained using only one specific S_1 minimum representing a single UV-induced process, it cannot reproduce the entire range of the recorded TA spectrum. Moreover, the $^1\pi\pi^*$ state of guanosine that is responsible for the ultrafast ballistic photorelaxation channel would be rather strongly emissive owing to the bright character.[22,26,56,57] Accordingly, it seems very unlikely that the puzzling longer-lived excited state having a very weak broadband emission could originate from the ballistic photorelaxation channels.

To further support our interpretation, we simulated the ESA spectrum (see Fig. S7 in the ESI†) for the S_1 ($n\pi^*$) minimum of **Guo** in the gas phase located without the explicit water molecule. The absorption maxima (380 and 490 nm) and lineshape for the latter structure strongly differ from the experimental spectra (Fig. 2), and thus it reinforces our hypothesis about the fingerprint of the excited-state chalcogen bonding complex in the recorded transient absorption band.

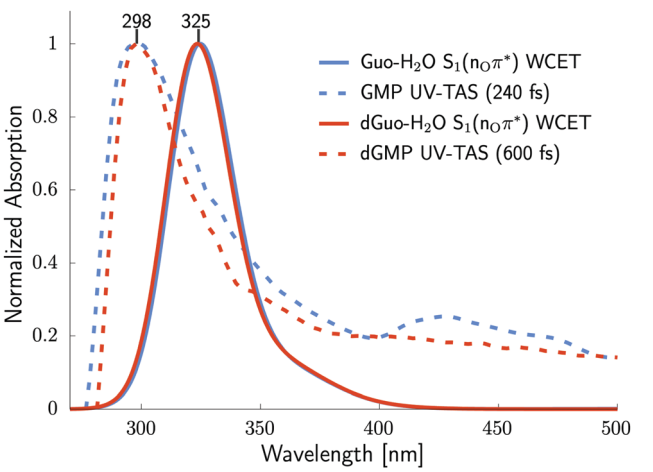

Fig. 2 The excited-state absorption (ESA) spectra were simulated using the SCS-ADC(2)/cc-pVTZ method, assuming the S_1 ($n_O\pi^*$) minimum-energy structures for **Guo-H_2O** (solid blue line) and **dGuo-H_2O** (solid red line) obtained at the SCS-ADC(2)/cc-pVTZ level. The digitalized experimental femtosecond transient absorption spectra of aqueous GMP (dashed blue line) and dGMP (dashed red line) recorded at 240 and 600 fs, respectively.[22,23]

Furthermore, dynamics of the bleaching band associated with the recovery of the electronic ground state of guanine nucleoside has the same lifetime (~2.0 ps) as the discussed transient absorption band (290–350 nm), which we assigned to the S_1 ($n_O\pi^*$) structure.[22,23] This shows that the $^1n_O\pi^*$ dark state can indeed be responsible for a large part of the photodynamics of guanine nucleosides, thus shedding an entirely new perspective on the aqueous photochemistry of heterocycles having a carbonyl group.

Methanol-to-chromophore electron transfer

In addition to the TR measurements in water, Cheng *et al.*[23] investigated also the photoinduced dynamics of deoxyguanosine in methanol. They observed that the lifetime of the transient absorption band (290–350 nm) and of the weak emission band (at 520 nm) increased to ~4.2 ps in this medium, when compared to the analogous bands in water.[23] This indicates that S_1 ($n_O\pi^*$) minimum is even more stabilized in methanol than in water.

To provide a mechanistic rationale for the TR measurements in methanol, we explored the $^1n_O\pi^*$ PE surface for a system containing deoxyguanosine and an explicit CH_3OH molecule (**dGuo-CH_3OH**) using the same SCS-ADC(2)/cc-pVTZ level of theory. We located a very similar S_1 minimum-energy structure having the C6–O···$OHCH_3$ chalcogen bonding interaction between **dGuo** and the methanol molecule (see Fig. 3 and Fig. S8 in the ESI†). The O···O distance at the S_1 minimum-energy geometry of **dGuo-CH_3OH** amounts to 2.07 Å (see Fig. S8 in ESI†) and the aromatic purine ring accepts 0.41 e^- from the explicit methanol molecule. The excited-state O···O chalcogen bond is noticeably shorter by 0.4 Å, and the associated charge transfer from the solvent molecule is roughly twice as large when compared to the S_1 minimum of the analogous **Guo-H_2O** complex. Importantly, the excited-state absorption (ESA) spectrum of the S_1 ($n_O\pi^*$) minimum of **dGuo-CH_3OH** (see Fig. S9 in ESI†) closely resembles the simulated ESA presented in Fig. 2 and is consistent with the transient absorption band (in the range of 290–350 nm) recorded in methanol.[23] Accordingly, methanol solvent molecules can stabilize the $^1n_O\pi^*$ excited state more strongly than water molecules, and as a result, the associated excited-state lifetime in methanol is doubled. Thus, excited-state chalcogen bonding between deoxyguanosine and methanol is now supported by both experimental[23] and theoretical results. It is worth adding that the S_1 ($n_O\pi^*$) minimum of the **dGuo-CH_3OH** complex was also reoptimized using the XMS-CASPT2/SA-CASSCF(10,9)/cc-pVDZ level of theory (see Fig. S8 in ESI†). The latter calculations confirmed the reliability of the excited-state interaction between the methanol molecule and deoxyguanosine.

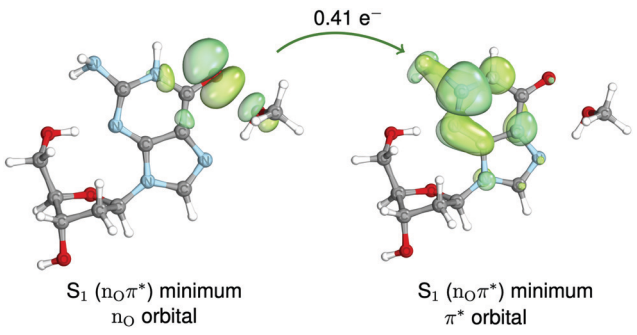

Fig. 3 The S_1 ($n_O\pi^*$) minimum-energy structure of **dGuo-CH_3OH** found at the SCS-ADC(2)/cc-pVTZ level of theory alongside the delocalized n_O and π^* molecular orbitals demonstrating a charge-transfer process of 0.41 e^- from CH_3OH to the nucleobase part.

Electron-driven proton transfer deactivation pathway

To elucidate the role of S_1 ($n_O\pi^*$) minimum (Fig. 1) in the photochemistry of guanine nucleosides, we located the relevant potential energy (PE) surface crossings and key structures at the SCS-ADC(2)/cc-pVTZ level of theory, and we present the associated potential energy profiles in Fig. 4.

Upon UV excitation of the $^1\pi\pi^*$ excited state (orange line), the system can readily reach the $^1\pi\pi^*/^1n_O\pi^*$ MECP at 4.74 eV (see the left inset in Fig. 4) that is marked by the elongation of the C6–O carbonyl bond (1.33 Å) as well as weakening of the C6–O···H_2O hydrogen bond (2.48 Å). Importantly, the located S_2/S_1 MECP shows that a slight elongation of the carbonyl bond by ~0.1 Å significantly stabilizes the energy of the $^1n_O\pi^*$ excited state with respect to the Franck–Condon region. The accessibility of S_2/S_1 MECP enables the population of the $^1n_O\pi^*$ excited state (blue line) and, in turn, the **Guo-H_2O** complex may reach the shallow S_1 minimum at 4.42 eV (shown in Fig. 1) in a barrierless manner.

The associated charge transfer found for the S_1 minimum-energy structure could trigger the electron-driven proton transfer (EDPT) from the water molecule to the N7 atom of guanosine. The EDPT mechanism having an energy barrier of 0.41 eV could then lead to S_1/S_0 MECP at 3.95 eV (see the right inset in Fig. 4), which allows for radiationless deactivation of guanosine. Notably, an energy barrier of 0.41 eV could be overcome due to excess excitation energy. Thus, the discussed

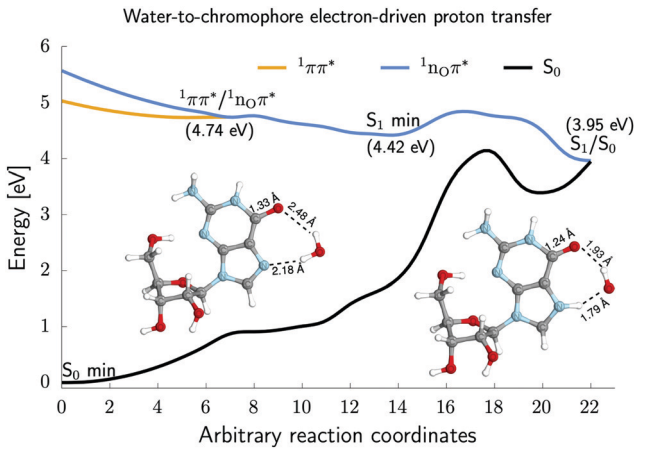

Fig. 4 The potential energy profiles (PE) demonstrate a photochemical channel, involving the S_2/S_1 minimum-energy crossing point (MECP), S_1 minimum, and S_1/S_0 MECP, that enables a water-to-chromophore electron-driven proton transfer (EDPT) mechanism in **Guo-H_2O**. The PE profiles were obtained at the SCS-ADC(2)/cc-pVTZ level of theory.

$^1n_O\pi^*$-mediated photorelaxation channel allows for a water-splitting process leading to the formation of hydrogenated guanosine radical and a hydroxyl ($^\bullet$OH) radical.

Benchmarking of relevant excited-state structures

Single reference *ab initio* methods such as SCS-ADC(2) are widely used to investigate photochemical processes, which occur in organic chromophores. However, Marsili *et al.*[60] have demonstrated that the ADC(2)-s method can lead to finding nonphysical S_1/S_0 surface crossings for carbonyl-containing compounds. To address a potential issue with applying the SCS-ADC(2) method to the excited-state optimization of **Guo-H$_2$O**, we reoptimized the SCS-ADC(2) $S_1(n_O\pi^*)$ minimum and the SCS-ADC(2) S_1 $(n_O\pi^*)/S_0$ minimum-energy crossing point using the XMS-CASPT2/SA-CASSCF(10,9)/cc-pVDZ level of theory. The molecular orbitals included in the complete active space for both excited-state structures are shown in the ESI† (Fig. S10 and S11).

The superimposed excited-state minimum-energy structures obtained at the SCS-ADC(2) (black) and XMS-CASPT2 (cyan) levels are depicted in Fig. 5. The root-mean-square deviations (RMSDs) evaluated for those structures amount to 0.082 and 0.135 Å for the S_1 minimum and S_1/S_0 surface crossing, respectively. This indicates that the geometries are virtually identical. Thus, the XMS-CASPT2 calculations confirmed that the excited-state structures provided by SCS-ADC(2) method are reliable.

Regarding the relevant structural parameters, the most significant difference between the S_1 minimum-energy geometries is found for the O$\cdots$O intermolecular distances that amount to 2.43 and 2.46 Å at the XMS-CASPT2 and SCS-ADC(2) levels, respectively. Furthermore, the C6–O bond length is shortened to 1.35 Å (by 0.05 Å) at the XMS-CASPT2 level in comparison with the SCS-ADC(2) geometry. Comparing XMS-CASPT2 and SCS-ADC(2) S_1/S_0 MECP, the noticeable structural difference is a slightly different position of the hydroxyl radical. Since the multireference method (XMS-CASPT2) predicted the excited-state O$\cdots$O intermolecular interaction and confirmed the existence of the electron-driven proton transfer S_1/S_0 surface crossing, we conclude that the SCS-ADC(2) method is suitable for the description of the electronic structure of our model system.

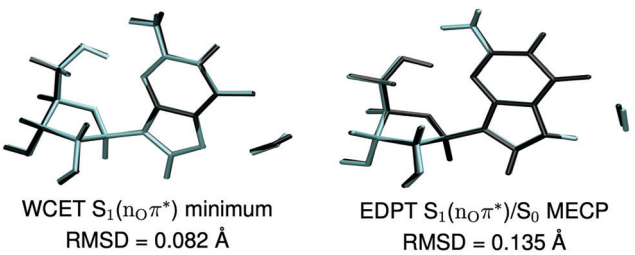

Fig. 5 The superimposed excited-state minimum-energy structures optimized at the SCS-ADC(2) S_1 minimum, SCS-ADC(2) S_1/S_0 surface crossing (black) and XMS-CASPT2/SA-CASSCF(10,9)/cc-pVDZ level (cyan) are presented with the root-mean-square deviation (RMSD) calculated for the corresponding structures.

Photolesions of guanine nucleosides

As described above, the EDPT photorelaxation mechanism generates two reactive radical species close to one another, that is, the $^\bullet$OH and **GuoH$^\bullet$** radicals, with the unpaired electron located on the C8 atom in the latter case. These radicals may readily recombine in the hot electronic ground state and produce a guanosine-OH (**Guo-OH**) photohydrate intermediate, the minimum-energy structure of which lies 1.96 eV (45.2 kcal mol^{-1}) below the EDPT S_1/S_0 minimum-energy crossing point (Fig. 6 and Fig. S12 in the ESI†). The vertical excitation energies calculated for the **Guo-OH** photohydrate (see Table 1) show that there is a low-lying $^1\pi\pi^*$ locally excited state at 4.08 eV having a substantial oscillator strength, which indicates that the photohydrate can easily absorb longer UV wavelengths (UV-B region) than the parent **Guo** molecule. In other words, the formation of **Guo** photohydrate redshifts the UV absorption spectrum of the chromophore and increases the photochemical activity of the molecule since it can be excited with much lower energies. More importantly, **Guo-OH** is also characterized by the low-lying $^1\pi\sigma^*$ excited state (at 4.23 eV, Table 1) that could enable the photodetachment of an electron from the intermediate, thus forming a radical cation that was previously proposed as the critical intermediate necessary for the formation of 8-oxo-guanosine.[13] Therefore, we propose that **Guo-OH** photohydrate could be the structural precursor of 8-oxo-guanosine, which is an important photolesion that can be formed in aqueous solution of guanine nucleosides.[13]

On the other hand, the main observed photoproduct upon UV excitation of guanosine in water is Fapy-guanosine (**Fapy-Guo**).[13] Given the above results, this may be explained by the C8–N9 bond rupture (see Fig. 6 and Fig. S12 in ESI†) of the **Guo-OH** photohydrate and subsequent proton transfer to the N9 atom, which allows for the formation of the more stable **Fapy-Guo**. Furthermore, the transition-state structure leading to the formation of **Fapy-Guo** is located 0.66 eV (15.2 kcal mol^{-1}, see Fig. S12 in ESI†) lower than the located S_1/S_0 minimum-energy crossing point. Consequently, photochemically formed and still vibrationally hot **Guo-OH** can be readily transformed to

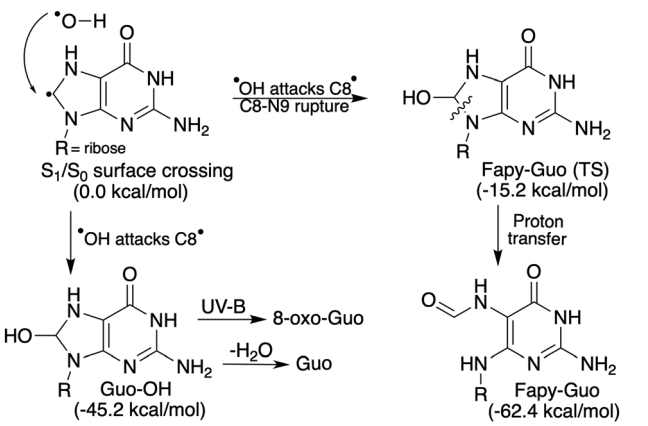

Fig. 6 Possible photoproducts generated from the biradical intermediate produced in the EDPT process, along with the relative energies of their ground-state structures with respect to EDPT S_1/S_0 state crossing.

Fapy-Guo after passing through this modest energy barrier. It is worth noting that the **Fapy-Guo** photoproduct is lower in energy than the EDPT S_1/S_0 surface crossing by 2.71 eV (62.4 kcal mol^{-1}). Interestingly, both **Fapy-Guo** and **Guo-H_2O** systems are nearly isoenergetic. We expect that **Fapy-Guo** should be a stable photoproduct that would not undergo a reverse ground-state conversion to **Guo**, particularly since such a reaction would involve a considerable energy barrier, exceeding 47.2 kcal mol^{-1} (*cf.* Fig. S12 in ESI†). The same photoproduct was also detected in the presence of electron scavengers (H_3O^+ and N_2O), suggesting that solvated electrons mediated by the $^1\pi\sigma^*$ state do not participate in the formation of **Fapy-Guo**.[13] This is consistent with our proposed mechanism for forming guanosine photolesions, which result from a direct water-to-chromophore electron transfer rather than the attachment of free solvated electrons to the chromophore.

Conclusions

In conclusion, we have demonstrated the long-sought plausible photochemical pathway leading to the formation of photolesions of aqueous guanine nucleosides, namely 8-oxo-guanosine and Fapy-guanosine. It involves the formation of an excited-state chalcogen bonded complex with a water molecule that enables the population and stabilization of the dark $^1n\pi^*$ state. This excited-state complex shows a substantial charge-transfer character, which can entail an electron-driven proton transfer process from a water molecule to the guanine ring leading to the formation of a reactive hydroxyl radical that may damage the canonical structure of guanine. The results of our quantum chemical calculations are strongly supported by reinterpretation of the time-resolved spectra recorded previously for aqueous guanine nucleosides, indicating that the intermolecular chalcogen bonding complex can be easily reached upon UV excitation. The proposed mechanism is the first that explains both the formation of **Fapy-Guo** as the main photoproduct in an aqueous solution and 8-oxo-guanine as a concomitant minor photoproduct. Furthermore, our results point out that the reactive dark $^1n\pi^*$ state, which seems to be hardly accessible owing to high excitation energy, can be substantially stabilized beyond the Franck–Condon region. This is in consequence of the formation of a specific and short-lived excited-state interaction that can lower the energy of the $n\pi^*$ state.

Our results also indicate that the SCS-ADC(2) method can be used as a more accurate alternative to the ADC(2)-s approach for studying the photochemical properties of carbonyl-containing compounds. However, we also strongly encourage benchmarking results of this single-reference method using multireference wavefunction methods, such as the XMS-CASPT2 level of theory.

Conflicts of interest

There are no conflicts to declare.

Acknowledgements

M. J. J. acknowledges the support of the 'Diamond Grant' (0144/DIA/2017/46) from the Polish Ministry of Science and Higher Education, a doctoral scholarship from the National Science Center Poland (2020/36/T/ST4/00564), and the START Fellowship from the Foundation for Polish Science. J. S. acknowledges support by the Czech Science Foundation (21-23718S) and the project SYMBIT reg. number: CZ.02.1.01/0.0/0.0/15_003/0000477 financed by the ERDF.

References

1 M. L. Kripke, P. A. Cox, L. G. Alas and D. B. Yarosh, *Proc. Natl. Acad. Sci. U. S. A.*, 1992, **89**, 7516–7520.
2 J. S. Taylor, *Acc. Chem. Res.*, 1994, **27**, 76–82.
3 V. Pagès and R. P. Fuchs, *Oncogene*, 2002, **21**, 8957–8966.
4 R. P. Sinha and D.-P. Häder, *Photochem. Photobiol. Sci.*, 2002, **1**, 225–236.
5 J. Cadet, E. Sage and T. Douki, *Mutat. Res.*, 2005, **571**, 3–17.
6 J. Cadet and J. R. Wagner, *Cold Spring Harbor Perspect. Biol.*, 2013, **5**, a012559.
7 J. Cadet and T. Douki, *Photochem. Photobiol. Sci.*, 2018, **17**, 1816–1841.
8 S. P. Jackson, *Carcinogenesis*, 2002, **23**, 687–696.
9 R. Madabhushi, L. Pan and L.-H. Tsai, *Neuron*, 2014, **83**, 266–282.
10 C. E. Crespo-Hernández, S. Flores, C. Torres, I. Negrón-Encarnación and R. Arce, *Photochem. Photobiol.*, 2000, **71**, 534–543.
11 C. E. Crespo-Hernández and R. Arce, *Photochem. Photobiol.*, 2000, **71**, 544–550.
12 G. A. Papadantonakis, R. Tranter, K. Brezinsky, Y. Yang, R. B. van Breemen and P. R. LeBreton, *J. Phys. Chem. B*, 2002, **106**, 7704–7712.
13 C. E. Crespo-Hernández and R. Arce, *J. Photochem. Photobiol., B*, 2004, **73**, 167–175.
14 M. Gomez-Mendoza, A. Banyasz, T. Douki, D. Markovitsi and J.-L. Ravanat, *J. Phys. Chem. Lett.*, 2016, **7**, 3945–3948.
15 D. B. Hall, R. E. Holmlin and J. K. Barton, *Nature*, 1996, **382**, 731–735.
16 W. J. Schreier, T. E. Schrader, F. O. Koller, P. Gilch, C. E. Crespo-Hernandez, V. N. Swaminathan, T. Carell, W. Zinth and B. Kohler, *Science*, 2007, **315**, 625–629.
17 K. V. Nguyen and C. J. Burrows, *J. Am. Chem. Soc.*, 2011, **133**, 14586–14589.
18 R. Szabla, J. Campos, J. E. Šponer, J. Šponer, R. W. Góra and J. D. Sutherland, *Chem. Sci.*, 2015, **6**, 2035–2043.
19 D. B. Bucher, C. L. Kufner, A. Schlueter, T. Carell and W. Zinth, *J. Am. Chem. Soc.*, 2016, **138**, 186–190.
20 R. Szabla, H. Kruse, P. Stadlbauer, J. Šponer and A. L. Sobolewski, *Chem. Sci.*, 2018, **9**, 3131–3140.
21 R. Szabla, M. Zdrowowicz, P. Spisz, N. J. Green, P. Stadlbauer, H. Kruse, J. Šponer and J. Rak, *Nat. Commun.*, 2021, **12**, 3018.

22 V. Karunakaran, K. Kleinermanns, R. Improta and S. A. Kovalenko, *J. Am. Chem. Soc.*, 2009, **131**, 5839–5850.
23 C. C.-W. Cheng, C. Ma, C. T.-L. Chan, K. Y.-F. Ho and W.-M. Kwok, *Photochem. Photobiol. Sci.*, 2013, **12**, 1351–1365.
24 D. A. McGovern, G. W. Doorley, A. M. Whelan, A. W. Parker, M. Towrie, J. M. Kelly and S. J. Quinn, *Photochem. Photobiol. Sci.*, 2009, **8**, 542–548.
25 J. B. Nielsen, J. Thøgersen, S. K. Jensen, S. B. Nielsen and S. R. Keiding, *Phys. Chem. Chem. Phys.*, 2011, **13**, 13821–13826.
26 S. F. Altavilla, J. Segarra-Martí, A. Nenov, I. Conti, I. Rivalta and M. Garavelli, *Front. Chem.*, 2015, **3**, 29.
27 S. E. Krul, S. J. Hoehn, K. J. Feierabend and C. E. Crespo-Hernández, *J. Chem. Phys.*, 2021, **154**, 075103.
28 J. Ortín-Fernández, J. González-Vázquez, L. Martínez-Fernández and I. Corral, *Molecules*, 2022, **27**, 989.
29 T. A. A. Oliver, Y. Zhang, A. Roy, M. N. R. Ashfold and S. E. Bradforth, *J. Phys. Chem. Lett.*, 2015, **6**, 4159–4164.
30 M. Barbatti, *J. Am. Chem. Soc.*, 2014, **136**, 10246–10249.
31 R. Szabla, H. Kruse, J. Šponer and R. W. Góra, *Phys. Chem. Chem. Phys.*, 2017, **19**, 17531–17537.
32 X. Wu, J. Ehrmaier, A. L. Sobolewski, T. N. V. Karsili and W. Domcke, *Phys. Chem. Chem. Phys.*, 2019, **21**, 14238–14249.
33 P. Pracht, F. Bohle and S. Grimme, *Phys. Chem. Chem. Phys.*, 2020, **22**, 7169–7192.
34 S. Grimme, *J. Chem. Theory Comput.*, 2019, **15**, 2847–2862.
35 J.-D. Chai and M. Head-Gordon, *Phys. Chem. Chem. Phys.*, 2008, **10**, 6615.
36 F. Weigend and R. Ahlrichs, *Phys. Chem. Chem. Phys.*, 2005, **7**, 3297–3305.
37 M. J. Frisch, G. W. Trucks, H. B. Schlegel, G. E. Scuseria, M. A. Robb, J. R. Cheeseman, G. Scalmani, V. Barone, G. A. Petersson, H. Nakatsuji, X. Li, M. Caricato, A. V. Marenich, J. Bloino, B. G. Janesko, R. Gomperts, B. Mennucci, H. P. Hratchian, J. V. Ortiz, A. F. Izmaylov, J. L. Sonnenberg, D. Williams-Young, F. Ding, F. Lipparini, F. Egidi, J. Goings, B. Peng, A. Petrone, T. Henderson, D. Ranasinghe, V. G. Zakrzewski, J. Gao, N. Rega, G. Zheng, W. Liang, M. Hada, M. Ehara, K. Toyota, R. Fukuda, J. Hasegawa, M. Ishida, T. Nakajima, Y. Honda, O. Kitao, H. Nakai, T. Vreven, K. Throssell, J. A. Montgomery Jr., J. E. Peralta, F. Ogliaro, M. J. Bearpark, J. J. Heyd, E. N. Brothers, K. N. Kudin, V. N. Staroverov, T. A. Keith, R. Kobayashi, J. Normand, K. Raghavachari, A. P. Rendell, J. C. Burant, S. S. Iyengar, J. Tomasi, M. Cossi, J. M. Millam, M. Klene, C. Adamo, R. Cammi, J. W. Ochterski, R. L. Martin, K. Morokuma, O. Farkas, J. B. Foresman and D. J. Fox, *Gaussian-16 Revision B.03*, 2016, Gaussian Inc., Wallingford CT.
38 A. Hellweg, S. A. Grün and C. Hättig, *Phys. Chem. Chem. Phys.*, 2008, **10**, 4119.
39 C. Hättig, *Adv. Quantum Chem.*, 2005, **50**, 37–60.
40 A. Dreuw and M. Wormit, *Wiley Interdiscip. Rev.: Comput. Mol. Sci.*, 2015, **5**, 82–95.
41 R. A. Kendall, T. H. Dunning and R. J. Harrison, *J. Chem. Phys.*, 1992, **96**, 6796–6806.
42 F. Plasser, *J. Chem. Phys.*, 2020, **152**, 084108.
43 B. G. Levine, J. D. Coe and T. J. Martínez, *J. Phys. Chem. B*, 2008, **112**, 405–413.
44 K. Andersson, P. A. Malmqvist, B. O. Roos, A. J. Sadlej and K. Wolinski, *J. Phys. Chem.*, 1990, **94**, 5483–5488.
45 T. Shiozaki, W. Györffy, P. Celani and H.-J. Werner, *J. Chem. Phys.*, 2011, **135**, 081106.
46 V. Veryazov, P. Å. Malmqvist and B. O. Roos, *Int. J. Quantum Chem.*, 2011, **111**, 3329–3338.
47 T. Shiozaki, *Wiley Interdiscip. Rev.: Comput. Mol. Sci.*, 2018, **8**, e1331.
48 TURBOMOLE V7.3 2018, a development of University of Karlsruhe and Forschungszentrum Karlsruhe GmbH, 1989-2007, TURBOMOLE GmbH, since 2007; available from http://www.turbomole.com.
49 N. M. O'boyle, A. L. Tenderholt and K. M. Langner, *J. Comput. Chem.*, 2008, **29**, 839–845.
50 S. Smidstrup, A. Pedersen, K. Stokbro and H. Jónsson, *J. Chem. Phys.*, 2014, **140**, 214106.
51 J. Zheng, X. Xu and D. G. Truhlar, *Theor. Chem. Acc.*, 2011, **128**, 295–305.
52 F. Neese, *Wiley Interdiscip. Rev.: Comput. Mol. Sci.*, 2012, **2**, 73–78.
53 D. Tuna, A. L. Sobolewski and W. Domcke, *J. Phys. Chem. A*, 2014, **118**, 122–127.
54 D. Tuna and W. Domcke, *Phys. Chem. Chem. Phys.*, 2016, **18**, 947–955.
55 L. Zhao, G. Zhou, B. Jia, G. Teng, K. Zhan, H. Zheng, J. Luo and B. Liu, *J. Photochem. Photobiol., A*, 2020, **401**, 112753.
56 L. Serrano-Andrés, M. Merchán and A. C. Borin, *J. Am. Chem. Soc.*, 2008, **130**, 2473–2484.
57 B. Heggen, Z. Lan and W. Thiel, *Phys. Chem. Chem. Phys.*, 2012, **14**, 8137–8146.
58 M. J. Janicki, R. Szabla, J. Šponer and R. W. Góra, *Chem. Phys.*, 2018, **515**, 502–508.
59 T. Fellowes, B. L. Harris and J. M. White, *Chem. Commun.*, 2020, **56**, 3313–3316.
60 E. Marsili, A. Prlj and B. F. E. Curchod, *Phys. Chem. Chem. Phys.*, 2021, **23**, 12945–12949.

